

Low-energy parameters and spin gap of a frustrated spin- s Heisenberg antiferromagnet with $s \leq \frac{3}{2}$ on the honeycomb lattice

R F Bishop and P H Y Li

School of Physics and Astronomy, Schuster Building, The University of Manchester, Manchester, M13 9PL, UK

School of Physics and Astronomy, University of Minnesota, 116 Church Street SE, Minneapolis, Minnesota 55455, USA

E-mail: raymond.bishop@manchester.ac.uk; peggyhyli@gmail.com

Abstract. The coupled cluster method is implemented at high orders of approximation to investigate the zero-temperature ($T = 0$) phase diagram of the frustrated spin- s J_1 - J_2 - J_3 antiferromagnet on the honeycomb lattice. The system has isotropic Heisenberg interactions of strength $J_1 > 0$, $J_2 > 0$ and $J_3 > 0$ between nearest-neighbour, next-nearest-neighbour and next-next-nearest-neighbour pairs of spins, respectively. We study it in the case $J_3 = J_2 \equiv \kappa J_1$, in the window $0 \leq \kappa \leq 1$ that contains the classical tricritical point (at $\kappa_{\text{cl}} = \frac{1}{2}$) of maximal frustration, appropriate to the limiting value $s \rightarrow \infty$ of the spin quantum number. We present results for the magnetic order parameter M , the triplet spin gap Δ , the spin stiffness ρ_s and the zero-field transverse magnetic susceptibility χ for the two collinear quasiclassical antiferromagnetic (AFM) phases with Néel and striped order, respectively. Results for M and Δ are given for the three cases $s = \frac{1}{2}$, $s = 1$ and $s = \frac{3}{2}$, while those for ρ_s and χ are given for the two cases $s = \frac{1}{2}$ and $s = 1$. On the basis of all these results we find that the spin- $\frac{1}{2}$ and spin-1 models both have an intermediate paramagnetic phase, with no discernible magnetic long-range order, between the two AFM phases in their $T = 0$ phase diagrams, while for $s > 1$ there is a direct transition between them. Accurate values are found for all of the associated quantum critical points. While the results also provide strong evidence for the intermediate phase being gapped for the case $s = \frac{1}{2}$, they are less conclusive for the case $s = 1$. On balance however, at least the transition in the latter case at the striped phase boundary seems to be to a gapped intermediate state.

1. Introduction

Extended, uniform spin-lattice models of quantum magnets comprise a number $N(\rightarrow \infty)$ of $SU(2)$ spins with a given spin quantum number s placed on the sites of a specified regular, periodic lattice in d dimensions. The interactions between the spins are typically modelled by pairwise Heisenberg exchange interactions with specified coupling strengths. Of particular interest in this context are models that exhibit both quasiclassical behaviour and nonclassical behaviour, typically with paramagnetic phases in some part of the relevant parameter space that do not exist for their classical counterparts (i.e., with $s \rightarrow \infty$), and which hence do not show magnetic long-range order (LRO).

Clearly, it is therefore especially advantageous to investigate models and situations in which quantum effects are enhanced. Broadly speaking, one expects that quantum fluctuations will be

greater in such spin-lattice systems where each of the spin quantum number s , the dimensionality d , and the coordination number z of the lattice take lower values. However, the well-known Mermin-Wagner theorem [1] prohibits all forms of magnetic LRO for systems with $d = 1$, even at zero temperature ($T = 0$), and for systems with $d = 2$ and $T \neq 0$, since for all such systems it is not possible to break a continuous symmetry, and all such quasiclassical states with magnetic LRO break both time-reversal symmetry and $SU(2)$ spin-rotation symmetry. Hence, two-dimensional (2D) models at $T = 0$ have come to occupy a key role in the study of quantum phase transitions (QPTs) [2, 3].

Since the honeycomb lattice has the lowest coordination number ($z = 3$) of all eleven 2D Archimedean lattices (i.e., those that comprise only regular polygons, possibly of different sorts, and with all sites equivalent to one another), spin-lattice models based on it have been the subject of intense interest in recent years. Prototypical such models that have been investigated are those in which the Hamiltonian includes only terms in which the spins at lattice sites i and j interact via an isotropic Heisenberg interaction of the form $J_{ij}\mathbf{s}_i \cdot \mathbf{s}_j$. Much attention has been focussed on the case when the exchange couplings J_{ij} are restricted to be between nearest-neighbour (NN) pairs, all with equal strength J_1 , next-nearest-neighbour (NNN) pairs, all with equal strength J_2 , and next-next-nearest-neighbour (NNNN) pairs, all with equal strength J_3 . Both the resulting so-called J_1 - J_2 - J_3 model and, particularly, the two special cases of it with $J_3 = 0$ and $J_3 = J_2$ have been extensively investigated with a wide variety of theoretical techniques. While frustrated such honeycomb lattice models with spins having $s = \frac{1}{2}$ have been particularly intensively studied [4–29], considerably less attention has been paid to their counterparts with $s > \frac{1}{2}$ [30–34].

Our main aim in the present work is to extend the study of such honeycomb-lattice models with $s \geq 1$, by applying to them the coupled cluster method (CCM) (see, e.g., Refs. [35–38]) implemented to high orders of approximation. The CCM has been shown to give results of unsurpassed accuracy to an extremely wide array of physical systems, including those in condensed matter physics, quantum chemistry, atomic and molecular physics, quantum optics and solid-state optoelectronics, and nuclear and subnuclear physics (and see, e.g., Refs. [35–56] and references cited therein). We note in particular that the CCM has already been applied with great success to a wide diversity of spin-lattice problems of interest in quantum magnetism (and see, e.g., Refs. [13, 19–23, 29, 32–34, 53–56] and references cited therein). These include specific applications [13, 21, 29, 33] to the model that we study further here, as discussed in more detail in Sec. 2.

The plan for the remainder of this paper is as follows. In Sec. 2 we first describe the model, including some of the pertinent results for both the classical ($s \rightarrow \infty$) and $s = \frac{1}{2}$ cases. The CCM is then briefly reviewed in Sec. 3, before we present in Sec. 4 our results using it for the particular cases $s = 1$ and $s = \frac{3}{2}$. In particular, we present results for the ground-state (GS) magnetic order parameter, the triplet spin gap, the GS spin stiffness and the GS zero-field transverse magnetic susceptibility. Finally, we conclude with a discussion of the results in Sec. 5.

2. The model

The Hamiltonian of the J_1 - J_2 - J_3 model on the honeycomb lattice is specified as

$$\begin{aligned}
 H &= J_1 \sum_{\langle i,j \rangle} \mathbf{s}_i \cdot \mathbf{s}_j + J_2 \sum_{\langle\langle i,k \rangle\rangle} \mathbf{s}_i \cdot \mathbf{s}_k + J_3 \sum_{\langle\langle\langle i,l \rangle\rangle\rangle} \mathbf{s}_i \cdot \mathbf{s}_l \\
 &\equiv J_1 h(x, y); \quad x \equiv J_2/J_1, \quad y \equiv J_3/J_1,
 \end{aligned}
 \tag{1}$$

where the operators $\mathbf{s}_i \equiv (s_i^x, s_i^y, s_i^z)$ are the usual $SU(2)$ quantum spin operators on lattice site i , with $\mathbf{s}_i^2 = s(s+1)\mathbf{1}$. We shall compare and contrast here the cases with $s = \frac{1}{2}$, $s = 1$ and

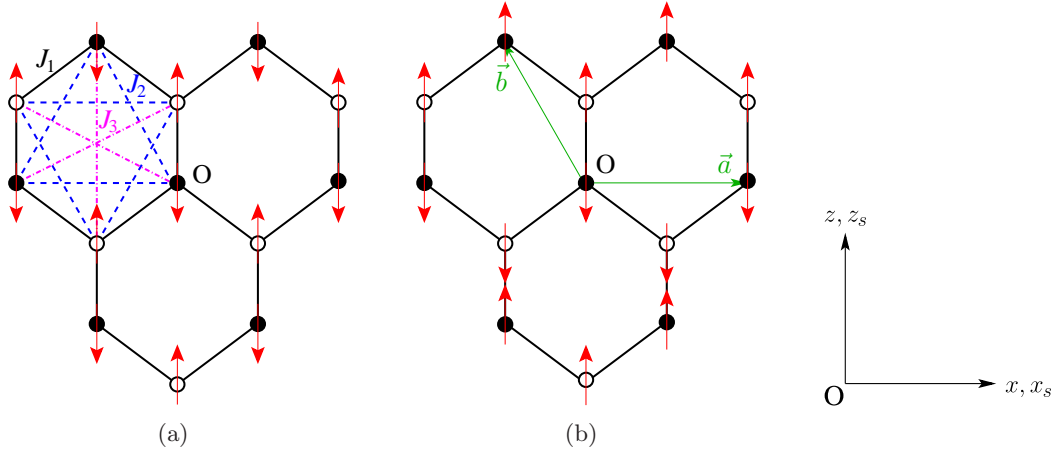


Figure 1. The J_1 - J_2 - J_3 honeycomb model with $J_1 > 0$; $J_2 > 0$; $J_3 > 0$, showing (a) the bonds ($J_1 = \text{—}$; $J_2 = \text{- - -}$; $J_3 = \text{- · -}$) and the Néel state, and (b) triangular Bravais lattice vectors \mathbf{a} and \mathbf{b} and one of the three equivalent striped states. Sites on sublattices \mathcal{A} and \mathcal{B} are shown by filled and empty circles respectively, and spins on the lattice are represented by the (red) arrows on the lattice sites. We also show both the lattice-plane axes (x, z) and the spin-space axes (x_s, z_s).

$s \geq \frac{3}{2}$. The sums in Eq. (1) over $\langle i, j \rangle$, $\langle\langle i, k \rangle\rangle$ and $\langle\langle\langle i, l \rangle\rangle\rangle$ run over all NN, NNN and NNNN bonds respectively, counting each bond once only in each sum. The lattice and the exchange bonds are illustrated in Fig. 1(a). We shall be interested in the present paper in the case when all three bonds are antiferromagnetic (AFM) (i.e., when $J_i > 0$; $i = 1, 2, 3$). The NN exchange coupling constant J_1 simply sets the overall energy scale, and hence the nontrivial parameters of the model may be taken as $J_2/J_1 \equiv x$ and $J_3/J_1 \equiv y$, so that we may rewrite the Hamiltonian as $H \equiv J_1 h(x, y)$, as in Eq. (1).

As we discuss in more detail below, the classical version ($s \rightarrow \infty$) of the model has a tricritical point at $x = y = \frac{1}{2}$ in its $T = 0$ phase diagram [4,6]). At this point the Hamiltonian may be rewritten in the particularly simple form

$$h\left(\frac{1}{2}, \frac{1}{2}\right) = \frac{1}{4} \sum_{\chi} \mathbf{s}_{\chi}^2 - \frac{3}{4} N s(s+1), \quad (2)$$

of a sum over edge-sharing hexagonal plaquettes χ , up to an additive constant term, where

$$\mathbf{s}_{\chi} = \sum_{i \in \chi} \mathbf{s}_i \quad (3)$$

is the total spin of the six spins on the elementary hexagon χ . Clearly, at this special point $x = y = \frac{1}{2}$, any state with zero total spin on each elementary hexagonal plaquette is a classical $T = 0$ GS phase, thereby giving rise to a macroscopic degeneracy. In fact, as we describe below, one of the three classical states with perfect magnetic LRO that emerges from this tricritical point, is itself also associated with an infinitely degenerate family (IDF) of GS phases. Indeed, this is one of the main reasons to be interested in the model, since classical spin-lattice systems that exhibit such an IDF of $T = 0$ GS phases are, *a priori*, prime candidates for the possible emergence of novel quantum phases (i.e., without classical counterparts) in the cases when the spin quantum number s is finite, since the role of quantum fluctuations is then, self-evidently, enhanced.

While the honeycomb lattice is bipartite (and hence not geometrically frustrated) it is non-Bravais. It comprises two sites per unit cell, with two triangular Bravais sublattices \mathcal{A} and \mathcal{B} . If we define the lattice to occupy the xz plane, the basis vectors may be chosen as $\mathbf{a} = \sqrt{3}d\hat{x}$ and $\mathbf{b} = \frac{1}{2}(-\sqrt{3}\hat{x} + 3\hat{z})d$, as illustrated in Fig. 1(b), where \hat{x} and \hat{z} are unit vectors in the x and z directions respectively, and d is the honeycomb lattice spacing (i.e., the distance between NN sites). The unit cell i residing at position vector $\mathbf{R}_i \equiv m_i\mathbf{a} + n_i\mathbf{b}$, with $m_i, n_i \in \mathbb{Z}$, contains the two sites at $\mathbf{R}_i \in \mathcal{A}$ and $(\mathbf{R}_i + d\hat{z}) \in \mathcal{B}$. The corresponding reciprocal lattice vectors are hence given by $\boldsymbol{\alpha} = 2\pi(\sqrt{3}\hat{x} + \hat{z})/(3d)$ and $\boldsymbol{\beta} = 4\pi/(3d)\hat{z}$. Thus, the first Brillouin zone and the Wigner-Seitz unit cell are the respective parallelograms formed by the pairs of vectors $(\boldsymbol{\alpha}, \boldsymbol{\beta})$ and (\mathbf{a}, \mathbf{b}) . Clearly, one may also take both as being centred on a point of sixfold rotational symmetry in their corresponding lattice planes. Thus, just as the Wigner-Seitz unit cell may be chosen to be bounded by the sides of an elementary hexagon (i.e., of side length d), as in Fig. 1, so the first Brillouin zone may also be chosen as a hexagon of side length $4\pi/(3\sqrt{3}d)$, which is rotated by 90° with respect to the Wigner-Seitz hexagon. Thus, the corners of the hexagon forming the first Brillouin zone are given by the vectors

$$\mathbf{K}^{(1)} = \frac{4\pi}{3\sqrt{3}d}\hat{x}, \quad \mathbf{K}^{(2)} = \frac{2\pi}{3\sqrt{3}d}(\hat{x} + \sqrt{3}\hat{z}), \quad \mathbf{K}^{(3)} = \frac{2\pi}{3\sqrt{3}d}(-\hat{x} + \sqrt{3}\hat{z}), \quad (4)$$

with the remaining three corners at positions $\mathbf{K}^{(i+3)} = -\mathbf{K}^{(i)}$; $i = 1, 2, 3$. Similarly, the mid-points of the edges of the first Brillouin zone have the vectors

$$\mathbf{M}^{(1)} = \frac{\pi}{3d}(\sqrt{3}\hat{x} + \hat{z}), \quad \mathbf{M}^{(2)} = \frac{2\pi}{3d}\hat{z}, \quad \mathbf{M}^{(3)} = \frac{\pi}{3d}(-\sqrt{3}\hat{x} + \hat{z}), \quad (5)$$

with the remaining three midpoints at positions $\mathbf{M}^{(i+3)} = -\mathbf{M}^{(i)}$; $i = 1, 2, 3$.

Returning now to the classical ($s \rightarrow \infty$) version of the model of Eq. (1), it has been shown [4,6] that its generic stable GS phase is described by a coplanar spiral configuration of spins. This may be defined, as usual, by a wave vector \mathbf{Q} , together with (for the non-Bravais two-site unit cell of the model) an angle ϕ that defines the relative orientation of the two sites in the same unit cell at position vector \mathbf{R}_i . The two classical spins in unit cell i thus have orientations

$$\mathbf{s}_{i,\sigma} = -s[\cos(\mathbf{Q} \cdot \mathbf{R}_i + \phi_\sigma)\hat{z}_s + \sin(\mathbf{Q} \cdot \mathbf{R}_i + \phi_\sigma)\hat{x}_s]; \quad \sigma = \mathcal{A}, \mathcal{B}, \quad (6)$$

where the spin-space plane is now defined by the two orthogonal unit vectors \hat{x}_s and \hat{z}_s , shown in Fig. 1. The two angles ϕ_σ are chosen so that $\phi_{\mathcal{A}} = 0$ and $\phi_{\mathcal{B}} = \phi$.

In the case considered here when all three bonds are AFM (i.e., with $J_1 > 0$, $x > 0$, $y > 0$), it has been shown [4,6] that the $T = 0$ classical GS phase diagram comprises three phases that meet at the tricritical point $(x, y) = (\frac{1}{2}, \frac{1}{2})$, discussed above. If we define our lattice origin to be at the centre of the hexagonal Wigner-Seitz unit cell, one may show that one value of the spiral wave vector \mathbf{Q} that minimizes the classical GS energy in this case is

$$\mathbf{Q} = \frac{2}{\sqrt{3}d} \cos^{-1} \left[\frac{(1-2x)}{4(x-y)} \right] \hat{x}, \quad (7)$$

together with the value $\phi = \pi$. Clearly, for Eq. (7) to be physically valid, we require $|(1-2x)/(x-y)| \leq 4$, or equivalently,

$$y \leq \frac{3}{2}x - \frac{1}{4}; \quad y \leq \frac{1}{2}x + \frac{1}{4}. \quad (8)$$

The two straight lines defined by Eq. (8) taken as equalities cross at the (tricritical) point $(x, y) = (\frac{1}{2}, \frac{1}{2})$. Along the first boundary line, $y = \frac{3}{2}x - \frac{1}{4}$, $\mathbf{Q} = \boldsymbol{\Gamma} = (0, 0)$, which (again,

together with the minimizing condition $\phi = \pi$) simply describes the Néel phase illustrated in Fig. 1(a). Similarly, everywhere along the second boundary line in Eq. (8), $y = \frac{1}{2}x + \frac{1}{4}$, we have $\mathbf{Q} = 2\pi/(\sqrt{3}d)\hat{x}$. In fact this vector lies outside the first Brillouin zone. When mapped back inside it takes the equivalent value $\mathbf{Q} = \mathbf{M}^{(2)}$, one of the midpoints of the edges of the hexagonal first Brillouin zone, given in Eq. (5). This wave vector (again together with the minimizing condition $\phi = 0$) describes the striped AFM phase illustrated in Fig. 1(b). It is clear that the phase transitions across the boundaries of Eq. (8) considered as equalities (i.e., between the Néel and spiral phases, and between the striped and spiral phases) are both continuous ones. One may also readily show from energetics that the phase transition between the two collinear AFM (Néel and striped) phases is of first-order type, and occurs along the boundary $x = \frac{1}{2}$, which again meets the other two phase boundaries at the classical tricritical point $(x, y) = (\frac{1}{2}, \frac{1}{2})$.

It is obvious that both the striped phase and the spiral phase described by Eq. (7) break the rotational symmetry and that there must be two other equivalent states in each case, obtained by a rotation of $\pm\frac{2}{3}\pi$ in the honeycomb xz plane. For the striped state this threefold degeneracy is simply equivalent to the wave vector \mathbf{Q} being allowed to take any of the position vectors $\mathbf{M}^{(i)}$; $i = 1, 2, 3$, of the three inequivalent midpoints of the sides of the hexagonal first Brillouin zone, as given by Eq. (5), together with $\phi = 0$ in the cases with $i = 1, 3$.

Although it is known [57] that classical GS spin configurations can generally be described as in Eq. (6), it is also known [57] that there are exceptional cases when the GS order is either not unique (up to a global rotation) or has a discrete degeneracy such as that associated with the striped state. Such exceptions are known [6, 57] to occur for special values of the ordering wave vector \mathbf{Q} . These include the cases when \mathbf{Q} takes a value equal to either one half or one quarter of a reciprocal lattice vector $\mathbf{G}_i \equiv k_i\boldsymbol{\alpha} + l_i\boldsymbol{\beta}$, with $k_i, l_i \in \mathbb{Z}$. The striped states are precisely of this form since their wave vectors $\mathbf{Q} = \mathbf{M}^{(i)}$, $i = 1, 2, 3$, are precisely one half of corresponding reciprocal lattice vectors, i.e., $\mathbf{M}^{(1)} = \frac{1}{2}\boldsymbol{\alpha}$, $\mathbf{M}^{(2)} = \frac{1}{2}\boldsymbol{\beta}$, $\mathbf{M}^{(3)} = \frac{1}{2}(\boldsymbol{\beta} - \boldsymbol{\alpha})$. In this case it has been explicitly shown [6] that the GS ordering has an IDF of non-planar spin configurations, all degenerate in energy with the collinear striped states. It has also been shown [4, 6] that, at least in the large- s limit when lowest-order spin-wave theory (LSWT) becomes exact, quantum fluctuations lift this degeneracy in favour of the AFM striped states, which now have the lowest energy.

To conclude our discussion of the classical limit ($s \rightarrow \infty$) of the J_1 - J_2 - J_3 model on the honeycomb lattice in the region where $J_1 > 0$, $x \geq 0$, $y \geq 0$, we have seen that at $T = 0$ its classical GS phase diagram has three phases, each with perfect magnetic LRO. These comprise (a) a Néel AFM phase in the region $y > 0$, $0 < x < \frac{1}{6}$ and $y > \frac{3}{2}x - \frac{1}{4}$, $\frac{1}{6} < x < \frac{1}{2}$; (b) a collinear striped AFM phase in the region $y > \frac{1}{2}x + \frac{1}{4}$, $x > \frac{1}{2}$; and (c) a coplanar spiral phase in the region $0 < y < \frac{3}{2}x - \frac{1}{4}$, $\frac{1}{6} < x < \frac{1}{2}$ and $0 < y < \frac{1}{2}x + \frac{1}{4}$, $x > \frac{1}{2}$. For a further discussion of the classical $T = 0$ GS phase diagram of the model, and for other exceptional cases (including those when \mathbf{Q} takes a value $\frac{1}{2}\mathbf{G}_i$ or $\frac{1}{4}\mathbf{G}_i$) the reader is referred to Refs. [6, 7, 33]. Although not of direct relevance here, the case $y = 0$ that includes a spiral phase for $x > \frac{1}{6}$, also includes a one-parameter IDF of incommensurate GS phases wherein the wave vector \mathbf{Q} can orient in an arbitrary direction, with degenerate solutions along a specific contour for a given value of x (and see Refs. [6, 7] for details). Again, at the level of LSWT, this degeneracy is lifted by quantum fluctuations to give spiral order by disorder.

The most interesting region of the classical phase diagram, for reasons discussed above, includes the tricritical point and the striped phase (that is part of an IDF of GS phases). Both are sampled along the line $y = x = \kappa$ (i.e., in the region $J_1 > 0$, $J_3 = J_2 \equiv \kappa J_1$, $\kappa > 0$). Hence, for the remainder of this study we work in this regime. Since the classical tricritical point is at $\kappa_{\text{cl}} = \frac{1}{2}$, we shall investigate specifically the window $0 \leq \kappa \leq 1$ of the frustration parameter.

For the case $s = \frac{1}{2}$, the model has been studied previously in the same parameter range

$0 \leq \kappa \leq 1$ [9, 13, 21, 29]. Each of these studies concurs on the finding that the classical transition at $\kappa_{cl} = \frac{1}{2}$ for the limiting case $s \rightarrow \infty$ is split into two transitions for the case $s = \frac{1}{2}$, one at $\kappa_{c_1} < \frac{1}{2}$ and the other at $\kappa_{c_2} > \frac{1}{2}$. Whereas LSWT provides the relatively crude estimates $\kappa_{c_1} \approx 0.29$ and $\kappa_{c_2} \approx 0.55$, the more powerful, and potentially more accurate method of Schwinger-boson mean-field theory (SBMFT) gives the estimates $\kappa_{c_1} \approx 0.41$ and $\kappa_{c_2} \approx 0.6$ [9]. These SBMFT calculations also predict a quantum disordered phase in the intermediate region $\kappa_{c_1} < \kappa < \kappa_{c_2}$, in which a gap in the bosonic dispersion opens up. These results are broadly confirmed by high-order CCM calculations [13, 21, 29], which yield the most accurate results to date for this case. From extensive calculations of a wide variety of low-energy parameters and the triplet spin gap for the model, the best CCM estimates are $\kappa_{c_1} = 0.45 \pm 0.02$ and $\kappa_{c_2} = 0.60 \pm 0.02$ [29]. Furthermore, CCM calculations of the plaquette valence-bond crystalline (PVBC) susceptibility [13] provide powerful evidence for the intermediate paramagnetic phase to be a gapped state with PVBC order over (almost all or) the entire region. Furthermore, very recently, the CCM has also been used to study a corresponding *AA*-stacked honeycomb bilayer model [58] for the case $s = \frac{1}{2}$, where each monolayer has the same bonds as here, but now with the addition of an AFM NN interlayer coupling, $J_1^\perp > 0$.

In view of these interesting results for the $s = \frac{1}{2}$ J_1 - J_2 - J_3 model with $J_3 = J_2$ and the known results for the classical limit ($s \rightarrow \infty$), it is clearly now intriguing also to consider the cases $s = 1$ and $s \geq 1$. The only results known to us are preliminary calculations of our own [33], again using the CCM. In that earlier work we calculated only the magnetic order parameter (out of the complete set of low-energy parameters) for the two AFM quasiclassical GS phases (i.e., the Néel and striped phases), for the cases $s = 1, \frac{3}{2}, 2, \frac{5}{2}$, as well as their PVBC susceptibilities. Based only on the vanishing of the magnetic order we found that the spin-1 case also had an intermediate non-classical phase, with Néel ordering now disappearing at $\kappa_{c_1} = 0.485 \pm 0.005$ and striped order disappearing at $\kappa_{c_2} = 0.528 \pm 0.005$. Just as for the $s = \frac{1}{2}$ case [13] it was also found for the $s = 1$ case [33] that the transition at κ_{c_1} appears to be of continuous type (and hence to be a candidate for deconfined quantum criticality [59, 60], since the Landau-Ginzburg-Wilson scenario cannot hold, as discussed in more detail in Ref. [13]), while that at κ_{c_2} appears to be of first-order type. Unlike in the $s = \frac{1}{2}$ case, however, where PVBC ordering seems to occur over the entire range $\kappa_{c_1} < \kappa < \kappa_{c_2}$, for the $s = 1$ case PVBC ordering appears to be absent everywhere (or, at most, to occur over only a very small part of the region). For all cases $s > 1$ studied in Ref. [33], but based only on calculations of the magnetic order parameter of the two AFM quasiclassical phases, the quantum phase diagram appears to be similar to the classical counterpart, i.e., with a direct first-order transition from the Néel to the striped phase, but with a critical value $\kappa_c(s)$ slightly greater than $\kappa_{cl} = \frac{1}{2}$. Thus, $\kappa_c(\frac{3}{2}) = 0.53 \pm 0.01$ and, for values $s > \frac{3}{2}$, $\kappa_c(s)$ appears to approach the classical value $\kappa_c(\infty) = 0.5$ monotonically as s is increased.

Our intention in the present paper is to add to these earlier preliminary findings for the model with $s > \frac{1}{2}$ by calculating for the cases $s = 1$ and $s = \frac{3}{2}$ both a complete set of GS low-energy parameters, to complement the calculations of the GS magnetic order parameter, and the triplet spin gap. In this sense we parallel the development of the $s = \frac{1}{2}$ version of the model, where the order parameter was first studied in Ref. [13], and only later were the more comprehensive calculations of a complete set of low-energy parameters and the triplet spin gap performed in Ref. [29]. Specifically, we will present results here in Sec. 4, again using high-order CCM calculations, for the spin stiffness coefficient ρ_s , the zero-field (uniform) transverse magnetic susceptibility χ , and the spin gap Δ .

3. The coupled cluster method

The CCM is nowadays regarded as providing one of the most accurate and most flexible *ab initio* techniques of modern microscopic quantum many-body theory (and see, e.g., Refs. [35–38]). The

method is size-extensive and size-consistent at all levels of approximate implementation. Hence, it can be utilized from the outset in the infinite system ($N \rightarrow \infty$) limit, thereby obviating the need for any finite-size scaling, such as is required by most competing methods, and hence circumventing any associated source of errors. Furthermore, the method also exactly preserves both the important Hellmann-Feynman theorem and the Goldstone linked cluster theorem at every level of approximation. These features ensure that the CCM provides accurate and self-consistent sets of results for a variety of both GS and excited-state (ES) parameters for the system under study. As is done here, the method can be implemented computationally to high orders of approximation within well-defined and well-understood truncation hierarchies, as outlined in more detail below. The results become exact as the order n of the truncation approaches infinity ($n \rightarrow \infty$), and hence the *sole* approximation ever made is to extrapolate the sequence of approximants that we calculate for any specific physical parameter.

By now the CCM has been applied to a very large number of spin-lattice systems, and we hence refer the reader to the extensive literature of such applications (and see, e.g., Refs. [29,33,34,53–56,58] and references cited therein) for full details. We content ourselves here with a very brief review of some of the most pertinent details connected with the present applications. A hallmark of the CCM is the incorporation of the quantum correlations present in the exact GS or ES wave functions via a very specific exponentiated form of correlation operator acting on an appropriately chosen model (or reference) state. For GS quantities, such as the energy and magnetic order parameter (i.e., the average local on-site magnetization) M , we use (separately) here both the Néel and striped states shown in Figs. 1(a) and 1(b), respectively, as our choices of model state. In order to calculate the lowest triplet ES energy gap Δ for the two quasiclassical phases, a spin-1 reference state is created from the above respective reference states by suitably exciting a single spin. For the calculations of the spin stiffness and magnetic susceptibility the above GS reference states have to be suitably modified by the imposition of a spin twist or a magnetic field, respectively, as we now outline in more detail.

Firstly, the spin stiffness ρ_s is a measure of the resistance of the system to an imposed rotation of the order parameter by an (infinitesimal) angle θ per unit length in a specific direction. If $E(\theta)$ is the GS energy as a function of the imposed twist, then

$$\frac{E(\theta)}{N} = \frac{E(\theta = 0)}{N} + \frac{1}{2}\rho_s\theta^2 + O(\theta^4), \quad (9)$$

where θ has the dimensions of inverse length. Clearly, magnetic LRO melts at the point where ρ_s vanishes. For the Néel state, whose ordering wave vector $\mathbf{Q} = \mathbf{\Gamma} = (0,0)$, clearly ρ_s is independent of the direction of the applied twist. By contrast, for the striped AFM state shown in Fig. 1(b), for which $\mathbf{Q} = 2\pi/(\sqrt{3}d)\hat{x}$, the relevant direction to apply the twist is the x direction. The corresponding twisted Néel and twisted striped states [29] are then used as CCM model states for the calculation of ρ_s in both GS phases. For the classical ($s \rightarrow \infty$) version of the AFM J_1 - J_2 - J_3 model under study on the honeycomb lattice, with $J_3 = J_2 \equiv \kappa J_1$, the definition of Eq. (9) easily leads to the corresponding classical values of ρ_s in the two AFM phases,

$$\rho_{s;\text{cl}}^{\text{Néel}} = \frac{3}{4}J_1(1 - 2\kappa)d^2s^2, \quad (10)$$

and

$$\rho_{s;\text{cl}}^{\text{striped}} = \frac{3}{4}J_1(-1 + 2\kappa)d^2s^2. \quad (11)$$

both of which are positive in the respective regions of stability of the two phases. As expected, the spin stiffness of the system vanishes precisely at the corresponding classical phase transition point, $\kappa_{\text{cl}} = \frac{1}{2}$.

Secondly, to calculate the transverse magnetic susceptibility when the system is aligned in either AFM phase in the spin-space z_s direction as in Fig. 1, we now place it in the transverse magnetic field $\mathbf{h} = h\hat{x}_s$. The Hamiltonian $H = H(h=0)$ of Eq. (1) then becomes modified to $H(h) = H(0) - h\sum_{k=1}^N s_k^x$, in units where the gyromagnetic ratio $g\mu_B/\hbar = 1$. The spins, which were previously aligned as in either Fig. 1(a) or Fig. 1(b), now cant at an angle $\phi = \phi(h)$ with respect to their zero-field configurations along the z_s direction. These corresponding canted Néel and canted striped states [29] are then used as CCM model states for the calculation of the respective transverse magnetic susceptibility, $\chi(h) = -N^{-1}d^2E/dh^2$, and its zero-field limit, $\chi = \chi(0)$, in which we are interested. In practice we calculate χ from

$$\frac{E(h)}{N} = \frac{E(h=0)}{N} - \frac{1}{2}\chi h^2 + O(h^4). \quad (12)$$

for some suitably small value of h . For the classical ($s \rightarrow \infty$) version of the AFM J_1 - J_2 - J_3 model under study on the honeycomb lattice, with $J_3 = J_2 \equiv \kappa J_1$, it is simple to calculate the canting angle $\phi(h)$ for the two quasiclassical AFM phases. The definition of Eq. (12) thus easily yields the corresponding classical values of χ for the two AFM phases,

$$\chi_{\text{cl}}^{\text{Néel}} = \frac{1}{6J_1(1+\kappa)}, \quad (13)$$

and

$$\chi_{\text{cl}}^{\text{striped}} = \frac{1}{2J_1(1+7\kappa)}, \quad (14)$$

where both parameters are independent of s at the classical level. We note that the two values become equal ($= \frac{1}{9}J_1^{-1}$), but nonzero, at the corresponding classical phase transition point, $\kappa_{\text{cl}} = \frac{1}{2}$.

We turn now to the choice of CCM approximation scheme. Once a suitable model state has been chosen, as outlined above, the approximation simply involves the choice of which multispin-flip configurations to retain in the CCM correlation operators. A rather general such approximation scheme is the so-called SUB m - n hierarchy [54]. At a given SUB m - n level one retains all multispin-flip configurations in the CCM correlation operators that involve m or fewer spin-flips spanning a range of no more than n contiguous sites on the lattice. Each single spin-flip is defined to require the action of a spin-raising operator $s_k^+ \equiv s_k^x + s_k^y$ acting once on the model ket state (in local spin axes chosen so that on each site a passive rotation has been performed to make each spin point downwards along the negative z_s axis). Furthermore, a set of lattice sites is defined to be contiguous if every site in the set is a NN (in a specified geometry) to at least one other member of the set. Clearly, as both indices m and n become infinite, the approximation becomes exact.

For spins with spin quantum number s , the maximum number of spin-flips per site, defined as above, is $2s$. Thus, when $m = 2sn$, the SUB m - n scheme becomes equivalent to the so-called localized lattice-animal-based subsystem (LSUB n) scheme in which all multispin-flip configurations in the CCM correlation operator expansions are retained that are defined over all distinct locales (or lattice animals in the usual graph-theoretic sense) on the lattice that comprise no more than n contiguous sites. Clearly, the LSUB $n \equiv$ SUB $2sn$ - n scheme is only equivalent to the SUB n - n scheme for the case $s = \frac{1}{2}$. In any such scheme we utilize the (space- and point-group) symmetries of both the system Hamiltonian and the CCM model state being used to reduce the set of independent multispin-flip configurations retained at any given order to a minimal number N_f . At a given n th level of LSUB n approximation, the number $N_f = N_f(n)$ is lowest for $s = \frac{1}{2}$ and increases sharply as a function of s . Because $N_f(n)$ also increases rapidly (typically super-exponentially) with the truncation index n , the most commonly used

CCM truncation hierarchy for spins $s > \frac{1}{2}$ is the SUB n - n scheme, and it is that scheme we employ here, just as in our previous work [33] on this model for cases with $s \geq 1$. In order to attain the higher values of the truncation index n necessary for high accuracy, we also use massively parallel supercomputing resources together with a specially tailored computer-algebra package [61] to derive and solve [53] the corresponding sets of CCM bra- and ket-state equations for both GS and ES quantities in the SUB n - n truncation scheme.

For the calculation of both the GS order parameter M and the ES gap parameter Δ we are restricted to SUB n - n calculations with $n \leq 12$ for the $s = \frac{1}{2}$ model and with $n \leq 10$ for the corresponding models with $s \geq 1$. For example, at the LSUB12 level for the calculation of M in the case $s = \frac{1}{2}$, we have $N_f(12) = 103\,097$ (250 891) when the Néel (striped) state is used as the CCM model state. For comparison, at the SUB10-10 level for calculations of M , we have corresponding numbers of fundamental configurations $N_f(10) = 219\,521$ (552 678) for the $s = 1$ model and $N_f(10) = 461\,115$ (1 207 202) for the corresponding $s = \frac{3}{2}$ model. Similarly at the LSUB12 level for the calculation of Δ for the spin- $\frac{1}{2}$ model, the corresponding numbers are $N_f(12) = 182\,714$ (465 196) based on the Néel (striped) state as CCM model state. For comparison, at the SUB10-10 level for calculations of Δ , we have $N_f(10) = 244\,533$ (642 054) for the spin-1 model and $N_f(10) = 418\,164$ (1 123 343) for the spin- $\frac{3}{2}$ model.

Due to the considerably reduced symmetries of both the twisted and canted model states in both quasiclassical phases, the corresponding SUB n - n calculations of ρ_s and χ can only be performed at orders $n \leq 10$ for the case $s = \frac{1}{2}$ and $n \leq 8$ for the cases $s \geq 1$. Thus, for example, at the LSUB10 level for the calculation of ρ_s in the case $s = \frac{1}{2}$, we have $N_f(10) = 347\,287$ when either the twisted Néel or the twisted striped state is used as the CCM model state. The corresponding number for ρ_s for the spin-1 model is $N_f(8) = 352\,515$ at the SUB8-8 level. Similarly, at the LSUB10 level for the calculation of χ for the spin- $\frac{1}{2}$ model, we have $N_f(10) = 58\,537$ (174 692) when the canted Néel (canted striped) state is used as the CCM model state. Corresponding numbers at the SUB8-8 level for χ for the spin-1 model are $N_f(8) = 59\,517$ (177 331).

As we have noted previously, once we have calculated CCM SUB n - n approximants for any physical parameter the *only* approximation that we ever make is the extrapolation to the (in principle) exact limit, $n \rightarrow \infty$. Although no exact such schemes are known theoretically, by now a great deal of practical experience has been built up from many applications to diverse models, so that we now have a uniform set of simple extrapolation rules, one for each parameter, that are applied consistently. For example, for highly frustrated spin-lattice models, particularly in cases where the system is close to a QCP or where the magnetic order parameter M is either zero or close to zero, a well-tested scaling scheme for M has been found (and see, e.g., Refs. [13, 19–23, 33, 34, 55, 56]) to be

$$M(n) = \mu_0 + \mu_1 n^{-1/2} + \mu_2 n^{-3/2}. \quad (15)$$

Similar such schemes for the spin gap, spin stiffness and zero-field transverse magnetic susceptibility all have a leading exponent of -1 (and see, e.g., Refs. [34, 56]),

$$\Delta(n) = d_0 + d_1 n^{-1} + d_2 n^{-2}, \quad (16)$$

$$\rho_s(n) = s_0 + s_1 n^{-1} + s_2 n^{-2}, \quad (17)$$

and

$$\chi(n) = x_0 + x_1 n^{-1} + x_2 n^{-2}. \quad (18)$$

Clearly, in order to extract the corresponding extrapolants μ_0 (for M), d_0 (for Δ), s_0 (for ρ_s) and x_0 (for χ) from Eqs. (15)–(18), respectively, we need to input at least three different corresponding SUB n - n approximants. Further details on the choice of such SUB n - n input sets are given in Sec. 4.

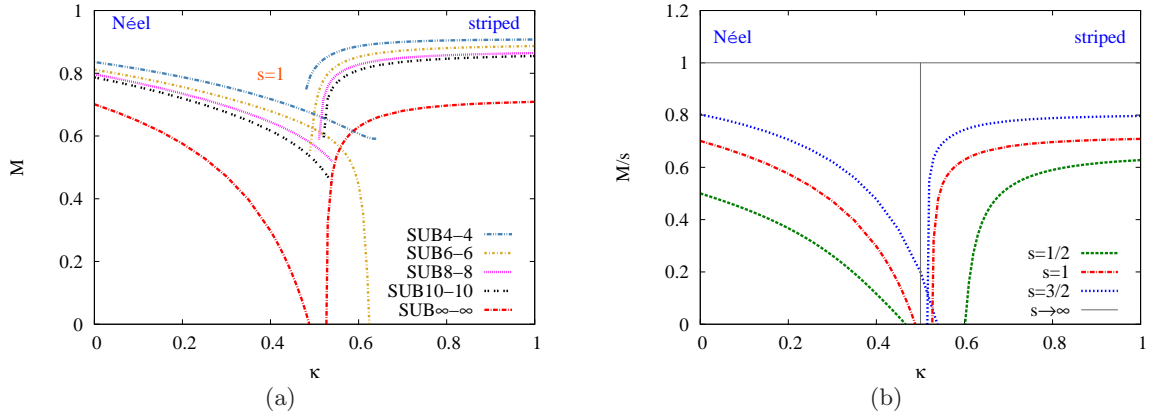


Figure 2. CCM results for the GS magnetic order parameter M for the J_1 - J_2 - J_3 model on the honeycomb lattice, with $J_1 > 0$ and $J_3 = J_2 \equiv \kappa J_1 > 0$, as a function of the frustration parameter κ , using both the Néel and striped states as the CCM model state. (a) Results are shown for the $s = 1$ case in $\text{SUB}n$ - n approximations with $n = 4, 6, 8, 10$, together with the respective $\text{SUB}\infty$ - ∞ extrapolant based on Eq. (15) and using this data set as input. (b) Extrapolated ($\text{SUB}\infty$ - ∞) results for M/s are shown for the three cases $s = \frac{1}{2}, 1, \frac{3}{2}$. In each case Eq. (15) has been used, together with the corresponding $\text{SUB}n$ - n data sets $n = \{6, 8, 10, 12\}$ for $s = \frac{1}{2}$ and $n = \{4, 6, 8, 10\}$ for $s = 1$ and $s = \frac{3}{2}$. The classical ($s \rightarrow \infty$) result is also shown.

4. Results

We first show in Fig. 2 our CCM results for the GS magnetic order parameter M . In Fig. 2(a) we consider the spin-1 case, where we show both the “raw” $\text{SUB}n$ - n data with $n = 4, 6, 8, 10$ (for the two cases where the CCM model state is chosen to be either the Néel state or the striped state) and the corresponding $n \rightarrow \infty$ ($\text{SUB}\infty$ - ∞) extrapolations based on Eq. (15) and using the $\text{SUB}n$ - n data set with $n = \{4, 6, 8, 10\}$ as input. One sees that the extrapolated Néel order parameter vanishes at a value $\kappa_{c_1} \approx 0.486$, while the extrapolated striped order parameter similarly vanishes at a value $\kappa_{c_2} \approx 0.527$. As is usually the case, the extrapolations are rather robust with respect to the choice of input data. For example, by comparing similar extrapolations using the alternative data sets with $n = \{4, 6, 8\}$ and $n = \{6, 8, 10\}$, and by making a more detailed error analysis of our results, we find that our best estimates for the QCPs of the spin-1 model are $\kappa_{c_1} = 0.485 \pm 0.005$ and $\kappa_{c_2} = 0.528 \pm 0.005$, as already quoted in Sec. 2. These may be compared with the corresponding best CCM estimates [29] of $\kappa_{c_1} = 0.45 \pm 0.02$ and $\kappa_{c_2} = 0.60 \pm 0.02$ for the QCPs of the spin- $\frac{1}{2}$ model.

We note from Fig. 2(a) that each of the $\text{SUB}n$ - n approximants for M terminates at some critical value of κ , beyond which no real solution can be found for the corresponding CCM equations. Such critical values depend both on the model state used and the order n of the $\text{SUB}n$ - n approximation. For the Néel state there is an upper such critical value, while for the striped state there is a corresponding lower critical value. These CCM termination points of the coupled sets of $\text{SUB}n$ - n equations are typical of the method and are very well understood. Thus, they are simply a reflection of the corresponding QCP that delimits the region of existence for the respective form of magnetic LRO pertaining to that of the CCM model state being used. For any specific finite value n of the $\text{SUB}n$ - n truncation index (and for a particular phase under study), Fig. 2(a) clearly demonstrates that the CCM solutions extend into the unphysical regime beyond the actual ($n \rightarrow \infty$) QCP out to the respective termination point. As the truncation index n is increased the extent of the corresponding unphysical regime shrinks, and ultimately disappears completely as $n \rightarrow \infty$ and the solution becomes exact.

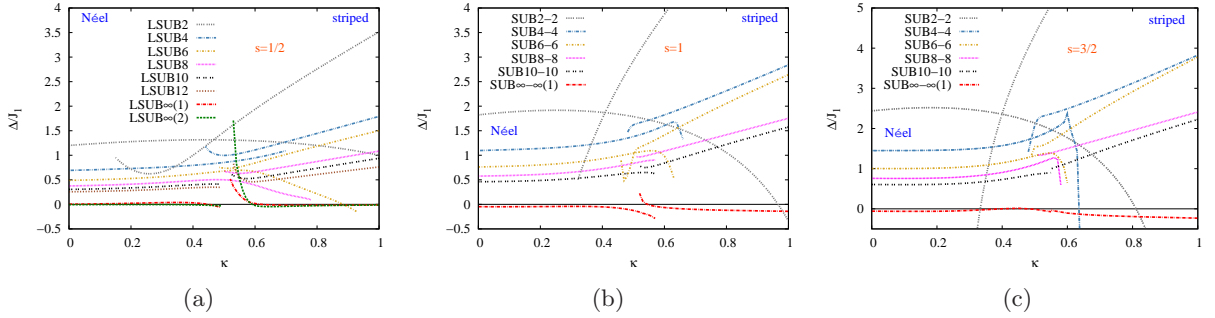


Figure 3. CCM results for the scaled triplet spin gap Δ/J_1 for the J_1 - J_2 - J_3 model on the honeycomb lattice, with $J_1 > 0$ and $J_3 = J_2 \equiv \kappa J_1 > 0$, as a function of the frustration parameter κ , using both the Néel and striped states as the CCM model state, for the three cases (a) $s = \frac{1}{2}$, (b) $s = 1$, and (c) $s = \frac{3}{2}$. Results are shown in $\text{SUB}n$ - n ($\equiv \text{LSUB}n$ for $s = \frac{1}{2}$ only) approximations with $n = 2, 4, 6, 8, 10$ in each case and also with $n = 12$ for the case $s = \frac{1}{2}$ only. Extrapolated $\text{SUB}\infty$ - $\infty(i)$ results are also shown, based in each case on Eq. (16) and the respective data sets $n = \{2, 6, 10\}$ for $i = 1$ and $n = \{4, 8, 12\}$ for $i = 2$ (in the case $s = \frac{1}{2}$ only).

The respective extrapolated CCM results for the scaled magnetic order parameter, M/s , for both the Néel and striped states are compared in Fig. 2(b) for the three cases $s = \frac{1}{2}$, $s = 1$ and $s = \frac{3}{2}$. Results for $s = 2$ and $s = \frac{5}{2}$ have also been given previously in Ref. [33]. One sees clearly that the evidence from our results for the magnetic order parameter alone is that the intermediate phase exists only for the two cases $s = \frac{1}{2}$ and $s = 1$. By contrast, for all cases $s \geq \frac{3}{2}$ the order parameter results indicate a direct transition between the Néel and striped phases at a QCP $\kappa_c(s)$, just as occurs classically in the $s \rightarrow \infty$ limit. For the case $s = \frac{3}{2}$ shown in Fig. 2(b), we find $\kappa_c(\frac{3}{2}) = 0.517 \pm 0.004$, based on the order parameter results alone. It has also been observed (and see Ref. [33] for further details) that $\kappa_c(s)$ appears to approach monotonically the classical value $\kappa_{\text{cl}} \equiv \kappa_c(\infty) = 0.5$ as s is increased further.

In order to provide further information about the QCPs observed from the magnetic order parameter results in Fig. 2, we now first turn our attention to the triplet spin gap Δ . We display our corresponding CCM results for Δ/J_1 as a function of κ in Figs. 3(a), 3(b) and 3(c) respectively for the three cases $s = \frac{1}{2}$, $s = 1$ and $s = \frac{3}{2}$. In each case raw $\text{SUB}n$ - n and extrapolated ($\text{SUB}\infty$ - ∞) results are shown based on both the Néel and striped collinear AFM states used separately as our CCM model state. Once again we observe termination points for the excited-state CCM equations, in complete analogy to those discussed above for the corresponding GS equations in connection with the magnetic order parameter results shown in Fig. 2.

At this point we should note that a $(4m - 2)/4m$ staggering effect, where $m \in \mathbb{Z}^+$ is a positive integer, has been observed previously [20, 23, 34, 58] in CCM $\text{SUB}n$ - n sequences of results (with n an even integer) for a variety of physical parameters on frustrated honeycomb lattices. Such staggering occurs when the $\text{SUB}n$ - n subsequence of results for some parameter with $n = (4m - 2)$ is differentially offset (or staggered) with respect to the corresponding subsequence with $n = 4m$. Both sub-sequences still obey an extrapolation scheme of the same sort (i.e., with the same leading exponent), but the coefficients are not identical for both cases. Such an effect is well known both in perturbation theory and in the CCM for all lattices as a corresponding $(2m - 1)/2m$ (i.e., odd/even) staggering. It is precisely for this reason that we do not show $\text{SUB}n$ - n results here also for odd values of n , since one should not mix odd and even sub-sequences in a single extrapolation. What is novel for honeycomb-lattice models is an *additional* staggering in the even-order series of terms for some physical observables between

those with $n = (4m - 2)$ and those with $n = 4m$. It has been postulated [34] that such an additional staggering can be attributed to the fact that the honeycomb lattice is non-Bravais, comprising two interlocking triangular Bravais lattices, on each of which the usual $(2m - 1)/2m$ staggering is observed.

While such a $(4m - 2)/4m$ staggering is not appreciable in the results shown in Fig. 2 for M , it is visibly apparent in the results shown in Fig. 3 for Δ , particularly in the striped phase, but also, albeit to a lesser extent, in the Néel phase. For this reason in our extrapolations for Δ based on Eq. (16) we take care not to mix SUB n - n terms in the input set with $n = (4m - 2)$ and those with $n = 4m$. Thus, for the case $s = \frac{1}{2}$ alone, shown in Fig. 3(a), where we have SUB n - n (\equiv LSUB n in this case) results with $n \leq 12$, we compare the extrapolation based on $n = \{2, 6, 10\}$ with that based on $n = \{4, 8, 12\}$. The agreement between the two is excellent in both stable quasiclassical phases, and again demonstrates the robustness of our extrapolation procedures. The only appreciable difference occurs precisely in the region of the intermediate paramagnetic state near to the boundary with the striped state. Since this is precisely the unphysical part of the region accessible with the striped CCM model state, it is where the associated errors are expected to be the largest and also the most difficult to estimate. What is clear, however, is that the evidence points strongly towards a gapped ($\Delta > 0$) state for the $s = \frac{1}{2}$ case in this intermediate region. For the corresponding cases with $s = 1$ and $s = \frac{3}{2}$ shown in Figs. 3(b) and 3(c) respectively, we are only able to perform SUB n - n calculations for Δ with $n \leq 10$. Hence, for these two cases, we only show the extrapolations for Δ based on Eq. (16) with the data set $n = \{2, 6, 10\}$ used as input.

It is very gratifying to note firstly from Fig. 3 that for both quasiclassical magnetic phases our extrapolated values for Δ are compatible with being zero, within very small numerical errors, over the ranges $\kappa < \kappa_{c1}$ and $\kappa > \kappa_{c2}$ (with QCPs at κ_{c1} and κ_{c2} as determined from Fig. 2 by the points where $M \rightarrow 0$) for the two cases $s = \frac{1}{2}$ and $s = 1$, and over the entire range $0 \leq \kappa \leq 1$ for the case $s = \frac{3}{2}$. This is exactly as expected for the case of magnetic LRO, where the low-energy magnon excitations are gapless. The very small negative values shown for parts of the quasiclassical regions in Fig. 3 are clearly just an artefact of the numerical extrapolations. Indeed, their magnitude gives us a good independent check on the overall level of accuracy of our results.

For the case $s = \frac{1}{2}$, shown in Fig. 3(a), there is clear evidence that in the intermediate paramagnetic regime the GS phase is gapped (i.e., with $\Delta > 0$), at least in the regime near κ_{c2} , where the excited-state LSUB n calculations based on the striped state as CCM model state extend considerably into the ‘‘unphysical regime’’ before the corresponding termination point (discussed previously for the GS solutions) is reached. By contrast, the excited-state LSUB n calculations based on the Néel state terminate for the higher values of n shown, and hence also for the LSUB $\infty(i)$ extrapolants, only just beyond the value κ_{c1} at which the Néel magnetic order parameter vanishes, as in Fig. 2. Correspondingly, it is more difficult, on the basis of the evidence from Δ alone, to state categorically that the intermediate state is gapped over the entire range $\kappa_{c1} < \kappa < \kappa_{c2}$ for the spin- $\frac{1}{2}$ model. Nevertheless, there is clear evidence that at the QCP κ_{c2} where the striped order melts, the emergent paramagnetic state *is* gapped, and that this gapped state persists over most (if not all) of the regime $\kappa_{c1} < \kappa < \kappa_{c2}$.

Turning next to the case $s = \frac{3}{2}$, shown in Fig. 3(c), it is clear that the extrapolant for Δ is zero (within numerical errors) over the entire range of values of the frustration parameter κ shown. For the highest-order SUB n - n calculations shown with $n = 10$, the two results, based separately on the Néel and striped states as CCM model states, terminate at essentially the same point. Furthermore, the two corresponding SUB10-10 results for Δ , shown in Fig. 3(c), lie on a single curve that is continuous and smooth, within very small uncertainties. The same is also true for the SUB ∞ - $\infty(1)$ extrapolant based on Eq. (16) and the input data set $n = \{2, 6, 10\}$. These results entirely corroborate our findings from Fig. 2 for the order parameter, that there

is a direct transition in the spin- $\frac{3}{2}$ case between the two quasiclassical collinear AFM states.

By contrast with the very clear results for Δ for both the $s = \frac{1}{2}$ case shown in Fig. 3(a) and the $s = \frac{3}{2}$ case shown in Fig. 3(c), the results in Fig. 3(b) for the $s = 1$ case are more open to interpretation. For example, in this case, even the two highest-order excited-state SUB n - n solutions shown (i.e., with $n = 10$), based separately on both the Néel and striped states as CCM model state, now show some (possibly unphysical) overlap region where both solutions exist. However, unlike the $s = \frac{3}{2}$ case, the two SUB10-10 solutions in this regime, while close to one another, do not smoothly overlap, as is also the case for the two corresponding SUB ∞ - ∞ (1) extrapolants. It seems unlikely that these differences can be attributed to numerical errors, although we cannot wholly rule this out. On balance, the evidence from the results in Fig. 3(b) for Δ , corroborate our finding from Fig. 2(b) that there is a small regime for the spin-1 model between the Néel and striped phases where the stable GS phase is paramagnetic. Furthermore, it also seems reasonably clear that near the QCP where this intermediate state meets the striped state, the former is also gapped, as in the spin- $\frac{1}{2}$ case. From Fig. 3(b) the point where the extrapolant shown for Δ becomes positive, viz., at $\kappa \approx 0.546$ is also very close to the value $\kappa_{c_2} \approx 0.528$ from Fig. 2(b) at which the striped magnetic LRO melts.

Finally, we turn our attention to the two remaining GS low-energy parameters (viz., the spin stiffness coefficient ρ_s and the zero-field transverse magnetic susceptibility χ). Since the results for the cases $s \geq \frac{3}{2}$ are already conclusive (i.e., that there is a direct first-order transition in each case between the Néel and striped AFM phases), we concentrate henceforward on comparing the two cases $s = \frac{1}{2}$ and $s = 1$. Due to the considerably reduced symmetries of both the twisted and canted (Néel and striped) CCM model states required to calculate ρ_s and χ , respectively, we are now only able to perform LSUB n calculations for $s = \frac{1}{2}$ with $n \leq 10$ and SUB n - n calculations for $s \geq 1$ with $n \leq 8$, for both parameters. This can be compared with the corresponding cases $n \leq 12$ and $n \leq 10$ respectively, for the calculations of M and Δ .

In Fig. 4 we display our CCM results for ρ_s (in units of $J_1 d^2$), using both the twisted Néel and twisted canted states separately as model states. The “raw” LSUB n results for the spin- $\frac{1}{2}$ case, shown in Fig. 4(a) are seen to be clearly different in character for the Néel state from their counterparts for the striped state. Thus, firstly, in the former case, the curves flatten and seem to acquire zero slope before or near their termination points, while the latter become steeper near their termination points. This is rather strong evidence for the QCP at κ_{c_1} where Néel order melts being of continuous type, while that at κ_{c_2} where striped order melts is of first-order type. Secondly, whereas the LSUB n results for the Néel state show no perceivable $(4m - 2)/4m$ staggering of the sort discussed above, such an effect is clearly seen in their counterparts for the striped state.

This latter difference is also clearly reflected in the behaviour of the extrapolated values. Thus, in Fig. 4(a) we display three different extrapolants LSUB ∞ (i), each of which is based on the scheme of Eq. (17), but using the three different input data sets $n = \{4, 6, 8\}$ for $i = 1$, $n = \{6, 8, 10\}$ for $i = 2$ and $n = \{2, 6, 10\}$ for $i = 3$. Clearly, for the Néel phase, the two extrapolants with $i = 1$ and $i = 2$ are nearly identical, thereby demonstrating both the lack of any appreciable $(4m - 2)/4m$ staggering and the robustness of our extrapolation procedure using Eq. (17). Interestingly, the only noticeable difference occurs in a very small region near κ_{c_1} where the LSUB ∞ (2) curve, which utilizes higher-order LSUB n approximants than the LSUB ∞ (1) curve (and which hence *a priori* is expected to be more accurate), now more closely reflects the continuous nature of the transition with ρ_s approaching zero with zero slope. Even so, the values for κ_{c_1} obtained from the two extrapolations, viz., $\kappa_{c_1} \approx 0.411$ from LSUB ∞ (1) and $\kappa_{c_1} \approx 0.433$ from LSUB ∞ (2), are in close agreement. By contrast, the two LSUB ∞ (i) extrapolants for the striped phase are not at all in agreement with one another for essentially all values of κ shown. This is clearly a reflection of the now marked $(4m - 2)/4m$ staggering, which is clearly perceived by visual inspection of the corresponding LSUB n curves, shown in

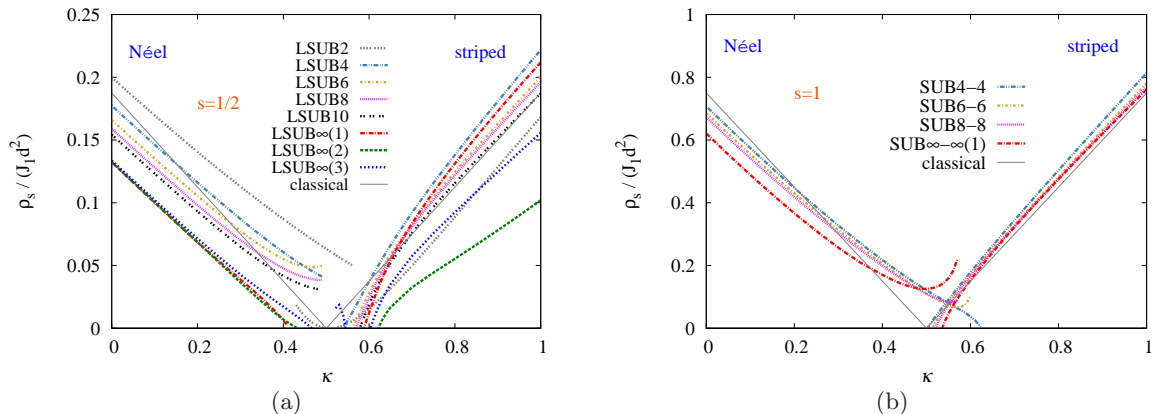


Figure 4. CCM results for the scaled spin stiffness $\rho_s/(J_1 d^2)$ for the J_1 - J_2 - J_3 model on the honeycomb lattice, with $J_1 > 0$ and $J_3 = J_2 \equiv \kappa J_1 > 0$, as a function of the frustration parameter κ , using both the twisted Néel and twisted striped states as the CCM model state, for the two cases (a) $s = \frac{1}{2}$ and (b) $s = 1$. Results are shown in SUB n - n (\equiv LSUB n for $s = \frac{1}{2}$ only) approximations with $n = 2, 4, 6, 8, 10$ for $s = \frac{1}{2}$ and $n = 4, 6, 8$ for $s = 1$. Extrapolated SUB ∞ - ∞ (i) results are also shown, based in each case on Eq. (17) and the respective data sets $n = \{4, 6, 8\}$ for $i = 1$, $n = \{6, 8, 10\}$ for $i = 2$ and $n = \{2, 6, 10\}$ for $i = 3$ (the latter two in the case $s = \frac{1}{2}$ only). The classical ($s \rightarrow \infty$) results from Eqs. (10) and (11) are also shown, using the values $s = \frac{1}{2}$ and $s = 1$ in panels (a) and (b), respectively.

Fig. 4(a), for the striped phase. The corresponding values now obtained for κ_{c_2} (i.e., the points where ρ_s for the striped phase vanishes) are $\kappa_{c_2} \approx 0.588$ from LSUB ∞ (1) and $\kappa_{c_2} \approx 0.621$ from LSUB ∞ (2).

Obviously, once such $(4m-2)/4m$ staggering effects have been detected, as above, one should base the extrapolations only on LSUB n subsequences with $n = (4m-2)$ alone or with $n = 4m$ alone. For the spin- $\frac{1}{2}$ case, where we have LSUB n results for ρ_s with $n \leq 10$, we can hence use an extrapolation based on Eq. (17) and input data set $n = \{2, 6, 10\}$, which should circumvent any complications of staggering. These are just the LSUB ∞ (3) results shown in Fig. 4(a). Again, on the Néel side, all three extrapolations are in good agreement with each other except close to the QCP at κ_{c_1} , whereas on the striped side the LSUB ∞ (3) curve should now be clearly taken as our preferred result. The corresponding locations of the two QCPs from the LSUB ∞ (3) extrapolation are $\kappa_{c_1} \approx 0.466$ and $\kappa_{c_2} \approx 0.603$. Both are in complete agreement with our previously quoted best CCM estimates [29] of $\kappa_{c_1} \approx 0.45 \pm 0.02$ and $\kappa_{c_2} \approx 0.60 \pm 0.02$.

Turning now to the corresponding spin-1 case, shown in Fig. 4(b), we only have SUB n - n results with $n \leq 8$, and hence we only display the SUB ∞ - ∞ (1) extrapolant based on Eq. (17) and the $n = \{4, 6, 8\}$ input data set. Clearly, on the Néel side the extrapolated value for ρ_s does not vanish, but instead displays a minimum at a value $\kappa \approx 0.495$. This is clearly a shortcoming of the extrapolation, which would presumably disappear if we had higher-order SUB n - n approximants available (e.g., with $n = 10$). Nevertheless, even this limited extrapolant is showing clear evidence for the corresponding QCP being continuous, just as in the spin- $\frac{1}{2}$ case. By contrast, on the striped side, where the QPT is of first-order type, the extrapolated result for ρ_s vanishes at a value $\kappa \approx 0.562$, in reasonable agreement with the previously quoted best CCM estimate [33] of $\kappa_{c_2} \approx 0.528 \pm 0.005$, obtained from the vanishing of the Néel order parameter. In summary, our present results for ρ_s for the spin-1 model reinforce our previous conclusions, while not adding significantly to their accuracy due to the fact that calculations for ρ_s can only be performed to lower orders (for comparable computing resources) than for M .

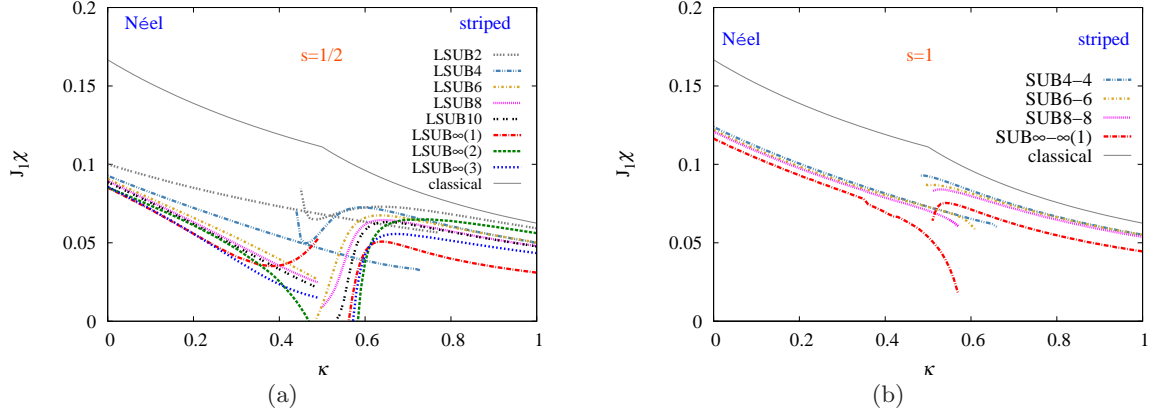


Figure 5. CCM results for the scaled zero-field, transverse magnetic susceptibility $J_1\chi$ for the J_1 - J_2 - J_3 model on the honeycomb lattice, with $J_1 > 0$ and $J_3 = J_2 \equiv \kappa J_1 > 0$, as a function of the frustration parameter κ , using both the canted Néel and canted striped states as the CCM model state, for the two cases (a) $s = \frac{1}{2}$ and (b) $s = 1$. Results are shown in SUB n - n (\equiv LSUB n for $s = \frac{1}{2}$ only) approximations with $n = 2, 4, 6, 8, 10$ for $s = \frac{1}{2}$ and $n = 4, 6, 8$ for $s = 1$. Extrapolated SUB ∞ - $\infty(i)$ results are also shown, based in each case on Eq. (18) and the respective data sets $n = \{4, 6, 8\}$ for $i = 1$, $n = \{6, 8, 10\}$ for $i = 2$ and $n = \{2, 6, 10\}$ for $i = 3$ (the latter two in the case $s = \frac{1}{2}$ only). The classical ($s \rightarrow \infty$) results from Eqs. (13) and (14) are also shown.

Finally, in Fig. 5, we show corresponding results for the zero-field transverse magnetic susceptibility χ to those shown in Fig. 4 for ρ_s . Two things are immediately apparent from Fig. 5. Firstly, it is evident that the effect of quantum fluctuations is to reduce χ in both quasiclassical AFM phases from its classical value. This reduction is greater for the spin- $\frac{1}{2}$ case than for the spin-1 case, as expected, but is considerable in both. Secondly, and more importantly, we observe from both Figs. 5(a) and 5(b) a marked tendency for χ to vanish at the two QCPs in each case. This is in marked contrast to the classical case where χ_{cl} , also shown in Fig. 5, takes a non-vanishing value ($= \frac{1}{9}$) at the corresponding single classical phase transition at $\kappa_{\text{cl}} = \frac{1}{2}$. Thus, in the classical case, when the spins are placed in a transverse magnetic field (of magnitude h) it is always energetically favourable to cant the spins, even in the limit $h \rightarrow 0$, and hence $\chi \equiv \chi(h = 0) \neq 0$. By contrast, in the case of a system of quantum spins, if the lowest available excited state has a nonzero excitation energy (i.e., $\Delta \neq 0$), no excitations are possible (at $T = 0$) as $h \rightarrow 0$. Hence, a positive signature of a spin gap opening up at any QCP at which quasiclassical magnetic LRO of any sort melts is the vanishing of χ there [62, 63], independent of the order of the transition.

Turning first to the spin- $\frac{1}{2}$ case, shown in Fig. 5(a), the results for χ show very similar effects (and explanations thereof) to those seen above in Fig. 4(a) for ρ_s . Thus, the shapes of the Néel and striped curves again reflect the different orders of their two transitions into the intermediate phase. Also, on the Néel side, the three extrapolations agree quite well with each other except near the QCP at κ_{c_1} . In particular, only for the LSUB ∞ (2) extrapolation, which employs solely the highest-order approximants available (i.e., those with $n = 6, 8, 10$) does χ vanish. The corresponding value $\kappa \approx 0.469$ at which χ vanishes is again in complete agreement with the best CCM estimate for κ_{c_1} (viz., $\kappa_{c_1} \approx 0.45 \pm 0.02$). Similarly to the results for ρ_s in Fig. 4(a), those in Fig. 5(a) for χ in the striped phase also show a marked $(4m - 2)/4m$ staggering effect, which is again reflected in the three shown LSUB ∞ (i) extrapolants. Corresponding points at which $\chi \rightarrow 0$ in the striped phase are, for example, $\kappa \approx 0.583$ for LSUB ∞ (2) and

$\kappa \approx 0.572$ for $\text{LSUB}_\infty(3)$, both in reasonable agreement with the best CCM estimate for κ_{c_2} (viz., $\kappa_{c_2} = 0.60 \pm 0.02$). Thus, the results for χ for the spin- $\frac{1}{2}$ case, like those for ρ_s , reinforce our earlier conclusions about its $T = 0$ phase diagram, while again not adding significantly to their accuracy for similar reasons. More importantly, however, they add considerable weight to our finding that the intermediate paramagnetic state is gapped over most (or all) of the region $\kappa_{c_1} < \kappa < \kappa_{c_2}$, particularly at and near the QCP at κ_{c_2} .

Finally, turning to the spin-1 case, shown in Fig. 5(b), we again only have SUB_{n-n} results for values of the truncation index $n \leq 8$, and hence we can only display the $\text{SUB}_{\infty-\infty}(1)$ extrapolant. Again, this has similar shortcomings to those discussed in relation to ρ_s for $s = 1$. While the extrapolated value for χ does not now vanish for either the Néel or striped phase, the tendency to do so is clear. Nevertheless, while these results for χ certainly do not contradict those in Fig. 3(b) for Δ for this case, the evidence for the intermediate state for the spin-1 model to be gapped remains weak at best, except possibly near the QCP at κ_{c_2} .

5. Discussion and conclusions

In this paper we have implemented the CCM to very high orders of approximation in order to investigate the frustrated spin- s J_1 - J_2 - J_3 Heisenberg antiferromagnet on the honeycomb monolayer lattice. We have concentrated on the case $J_3 = J_2 \equiv \kappa J_1$ and have investigated the $T = 0$ quantum phase diagrams of the model for various values of the spin quantum number s . In particular, we have investigated the phase structure of the model in the most interesting window $0 \leq \kappa \leq 1$ of the frustration parameter κ . This includes the classical tricritical point at $\kappa_{\text{cl}} = \frac{1}{2}$ of the full J_1 - J_2 - J_3 model, which is the point of maximum frustration. The classical model is the limiting case $s \rightarrow \infty$, and along the line $J_3 = J_2 \equiv \kappa J_1$ under study the system undergoes a single GS phase transition at $T = 0$, such that for $\kappa < \frac{1}{2}$ the stable phase has AFM Néel LRO, and for $\kappa > \frac{1}{2}$ there exists an IDF of non-planar spin configurations, all degenerate in energy, which includes the collinear state with AFM striped LRO as a special case. Both thermal and leading-order quantum fluctuations at $O(1/s)$ lift the degeneracy in favour of the striped state for $\kappa > \frac{1}{2}$. Our interest here has been to study whether and how quantum fluctuations change the structure of the classical phase diagram for various values of the spin quantum number s .

In order to do so we have first calculated very accurate values for the magnetic order parameter M of both quasiclassical AFM phases for a variety of values of the spin quantum number s . Clear evidence thereby emerged that for the two values $s = \frac{1}{2}$ and $s = 1$ the single classical critical point at $\kappa_{\text{cl}} = \frac{1}{2}$ is split into two QCPs, $\kappa_{c_1} < \kappa_{\text{cl}}$ and $\kappa_{c_2} > \kappa_{\text{cl}}$, such that the system maintains Néel magnetic LRO for $\kappa < \kappa_{c_1}$ and striped magnetic LRO for $\kappa > \kappa_{c_2}$, while the stable GS phase is a paramagnet, with no discernible magnetic LRO, in the intermediate regime $\kappa_{c_1} < \kappa < \kappa_{c_2}$. Our best estimates for the QCPs are $\kappa_{c_1} = 0.45 \pm 0.02$ and $\kappa_{c_2} = 0.60 \pm 0.02$ for the spin- $\frac{1}{2}$ model, and $\kappa_{c_1} = 0.485 \pm 0.005$ and $\kappa_{c_2} = 0.528 \pm 0.005$ for the spin-1 model. By contrast, for all values $s \geq \frac{3}{2}$, the results for M clearly indicate a direct first-order transition between the collinear Néel and striped AFM phases, at a value $\kappa_c(s)$ of the frustration parameter that depends on s and which appears to approach the classical value $\kappa_c(\infty) \equiv \kappa_{\text{cl}} = \frac{1}{2}$ monotonically from above. For example, for the spin- $\frac{3}{2}$ model we found $\kappa_c(\frac{3}{2}) \approx 0.517$.

Those findings from the behaviour of $M = M(\kappa)$ were reinforced from further high-order CCM calculations of the triplet spin gap Δ for the three cases $s = \frac{1}{2}, 1, \frac{3}{2}$. In particular, for the spin- $\frac{3}{2}$ model, our results showed that $\Delta = 0$, within very small numerical errors associated with the extrapolations, over the entire range $0 \leq \kappa \leq 1$, compatible with the existence therein everywhere of states with magnetic LRO, whose lowest-lying magnon excitations are gapless. By contrast, for the spin- $\frac{1}{2}$ model, clear evidence emerged that $\Delta \neq 0$ over at least a large part (if not all) of the intermediate regime $\kappa_{c_1} < \kappa < \kappa_{c_2}$ (especially near the second QCP at κ_{c_2}), fully compatible with earlier CCM finding [13] that the paramagnetic state in this case has PVBC order. For the remaining case, $s = 1$, the results from Δ were far less conclusive. Nevertheless,

on balance, the evidence does point towards a gapped state opening up at (or very near to) the QCP at κ_{c_2} at which striped order melts.

In view of these results we decided finally to calculate the remaining two low-energy parameters (viz., the spin stiffness ρ_s and the zero-field uniform transverse magnetic susceptibility χ). We decided also to focus on the two cases $s = \frac{1}{2}, 1$ in order to see if we could glean any further evidence from these parameters about the $T = 0$ quantum phase diagram of the spin-1 model, by comparing their behaviours as functions of κ with those of their spin- $\frac{1}{2}$ counterpart. For both cases $s = \frac{1}{2}$ and $s = 1$ the results and conclusions from the calculations of ρ_s largely supported those from the corresponding calculations of M . In particular, from the behaviour of the two curves $M = M(\kappa)$ and $\rho_s = \rho_s(\kappa)$ for both magnetically ordered phases, the evidence is that for both the spin- $\frac{1}{2}$ and the spin-1 model the transition at κ_{c_1} is continuous, while that at κ_{c_2} is first-order.

In principle, calculations of χ can be particularly illuminating since they can provide direct evidence of a gapped state opening, viz., at points where $\chi \rightarrow 0$. In the case of the spin- $\frac{1}{2}$ model the evidence was rather compelling that at both QCPs, κ_{c_1} and κ_{c_2} , χ vanishes, thereby reinforcing the belief that the intermediate state in this case is gapped everywhere, compatible with it having PVBC order over the whole intermediate interval $\kappa_{c_1} < \kappa < \kappa_{c_2}$. By contrast, for the spin-1 model the evidence was less conclusive, largely due to the fact that the previously known $(4m - 2)/4m$ staggering for CCM SUB n - n approximants of physical observables for honeycomb-lattice systems is clearly present for χ . Hence, this makes extrapolations of χ particularly problematic for the spin-1 model where SUB n - n approximants to χ are only really practicable (even with large amounts of supercomputing resources available, as here) for values $n \leq 8$ of the truncation parameter, in comparison with $n \leq 10$ for its spin- $\frac{1}{2}$ counterpart.

In summary, the $T = 0$ quantum phase diagrams for the model under study are now well understood from our CCM calculations for all values of the spin quantum number, except $s = 1$. The nature of the intermediate phase for the spin-1 model remains elusive, even after such an exhaustive study as has been performed here. While we have obtained weak evidence that a gapped state opens up as striped order vanishes below κ_{c_2} , this is far from being compelling. Furthermore, there is no direct evidence at all for a gapped state opening above κ_{c_1} where Néel order melts. It would clearly be of great interest to perform SUB10-10 calculations for χ in both magnetic phases for the case $s = 1$, although it seems infeasible that these will become available in the near future. It might also be of interest to use other alternative techniques for the spin-1 model, although they will clearly require very high accuracy to be able to give solid conclusions, on the evidence of the present work.

Acknowledgments

We thank the University of Minnesota Supercomputing Institute for the grant of supercomputing facilities, on which the work reported here was performed. One of us (RFB) gratefully acknowledges Leverhulme Trust for the award of an Emeritus Fellowship (EM-2015-007).

References

- [1] Mermin N D and Wagner H 1966 *Phys. Rev. Lett.* **17** 1133–1136
- [2] Sachdev S 2008 *Nat. Phys.* **4** 173–185
- [3] Sachdev S 2011 *Quantum Phase Transitions* 2nd ed (Cambridge, UK: Cambridge University Press)
- [4] Rastelli E, Tassi A and Reatto L 1979 *Physica B & C* **97** 1–24
- [5] Mattsson A, Fröjdh P and Einarsson T 1994 *Phys. Rev. B* **49** 3997–4002
- [6] Fouet J B, Sindzingre P and Lhuillier C 2001 *Eur. Phys. J. B* **20** 241–254
- [7] Mulder A, Ganesh R, Capriotti L and Paramekanti A 2010 *Phys. Rev. B* **81** 214419
- [8] Wang F 2010 *Phys. Rev. B* **82** 024419
- [9] Cabra D C, Lamas C A and Rosales H D 2011 *Phys. Rev. B* **83** 094506
- [10] Ganesh R, Sheng D N, Kim Y J and Paramekanti A 2011 *Phys. Rev. B* **83** 144414

- [11] Ganesh R, Sheng D N, Kim Y J and Paramekanti A 2011 *Phys. Rev. B* **83** 219903(E)
- [12] Clark B K, Abanin D A and Sondhi S L 2011 *Phys. Rev. Lett.* **107** 087204
- [13] Farnell D J J, Bishop R F, Li P H Y, Richter J and Campbell C E 2011 *Phys. Rev. B* **84** 012403
- [14] Reuther J, Abanin D A and Thomale R 2011 *Phys. Rev. B* **84** 014417
- [15] Albuquerque A F, Schwandt D, Hetényi B, Capponi S, Mambrini M and Läuchli A M 2011 *Phys. Rev. B* **84** 024406
- [16] Mosadeq H, Shahbazi F and Jafari S A 2011 *J. Phys.: Condens. Matter* **23** 226006
- [17] Oitmaa J and Singh R R P 2011 *Phys. Rev. B* **84** 094424
- [18] Mezzacapo F and Boninsegni M 2012 *Phys. Rev. B* **85** 060402(R)
- [19] Li P H Y, Bishop R F, Farnell D J J, Richter J and Campbell C E 2012 *Phys. Rev. B* **85** 085115
- [20] Bishop R F, Li P H Y, Farnell D J J and Campbell C E 2012 *J. Phys.: Condens. Matter* **24** 236002
- [21] Bishop R F and Li P H Y 2012 *Phys. Rev. B* **85** 155135
- [22] Li P H Y, Bishop R F, Farnell D J J and Campbell C E 2012 *Phys. Rev. B* **86** 144404
- [23] Bishop R F, Li P H Y and Campbell C E 2013 *J. Phys.: Condens. Matter* **25** 306002
- [24] Ganesh R, van den Brink J and Nishimoto S 2013 *Phys. Rev. Lett.* **110** 127203
- [25] Zhu Z, Huse D A and White S R 2013 *Phys. Rev. Lett.* **110** 127205
- [26] Zhang H and Lamas C A 2013 *Phys. Rev. B* **87** 024415
- [27] Gong S S, Sheng D N, Motrunich O I and Fisher M P A 2013 *Phys. Rev. B* **88** 165138
- [28] Yu X L, Liu D Y, Li P and Zou L J 2014 *Physica E* **59** 41–49
- [29] Bishop R F, Li P H Y, Götze O, Richter J and Campbell C E 2015 *Phys. Rev. B* **92** 224434
- [30] Zhao H H, Xu C, Chen Q N, Wei Z C, Qin M P, Zhang G M and Xiang T 2012 *Phys. Rev. B* **85** 134416
- [31] Gong S S, Zhu W and Sheng D N 2015 *Phys. Rev. B* **92** 195110
- [32] Bishop R F and Li P H Y 2016 *J. Magn. Magn. Mater.* **407** 348–357
- [33] Li P H Y, Bishop R F and Campbell C E 2016 *J. Phys.: Conf. Ser.* **702** 012001
- [34] Li P H Y and Bishop R F 2016 *Phys. Rev. B* **93** 214438
- [35] Bishop R F and Kümmel H G 1987 *Phys. Today* **40(3)** 52–60
- [36] Bishop R F 1991 *Theor. Chim. Acta* **80** 95–148
- [37] Bishop R F 1998 *Microscopic Quantum Many-Body Theories and Their Applications* Lecture Notes in Physics Vol. 510 ed Navarro J and Polls A (Berlin: Springer-Verlag) pp 1–70
- [38] Bartlett R J and Musiał M 2007 *Rev. Mod. Phys.* **79** 291–352
- [39] Coester F 1958 *Nucl. Phys.* **7** 421–424
- [40] Coester F and Kümmel H 1960 *Nucl. Phys.* **17** 477–485
- [41] Čížek J 1966 *J. Chem. Phys.* **45** 4256–4266
- [42] Čížek J 1969 *Adv. Chem. Phys.* **14** 35–89
- [43] Bishop R F and Lührmann K H 1978 *Phys. Rev. B* **17** 3757–3780
- [44] Kümmel H, Lührmann K H and Zabolitzky J G 1978 *Phys. Rep.* **36** 1–63
- [45] Bishop R F and Lührmann K H 1982 *Phys. Rev. B* **26** 5523–5557
- [46] Arponen J 1983 *Ann. Phys. (N.Y.)* **151** 311–382
- [47] Arponen J S, Bishop R F and Pajanne E 1987 *Phys. Rev. A* **36** 2519–2538
- [48] Arponen J S, Bishop R F and Pajanne E 1987 *Phys. Rev. A* **36** 2539–2549
- [49] Arponen J S and Bishop R F 1991 *Ann. Phys. (N.Y.)* **207** 171–217
- [50] Stanton J F and Bartlett R J 1993 *J. Chem. Phys.* **98** 7029–7039
- [51] Arponen J S and Bishop R F 1993 *Ann. Phys. (N.Y.)* **227** 275–333
- [52] Arponen J S and Bishop R F 1993 *Ann. Phys. (N.Y.)* **227** 334–380
- [53] Zeng C, Farnell D J J and Bishop R F 1998 *J. Stat. Phys.* **90** 327–361
- [54] Farnell D J J and Bishop R F 2004 *Quantum Magnetism* Lecture Notes in Physics Vol. 645 ed Schollwöck U, Richter J, Farnell D J J and Bishop R F (Berlin: Springer-Verlag) pp 307–348
- [55] Bishop R F, Li P H Y and Campbell C E 2014 *AIP Conf. Proc.* **1619** 40–50
- [56] Bishop R F, Li P H Y, Zinke R, Darradi R, Richter J, Farnell D J J and Schulenburg J 2017 *J. Magn. Magn. Mater.* **428** 178–188
- [57] Villain J 1977 *J. Phys. (France)* **38** 385–391
- [58] Bishop R F and Li P H Y 2017 *Phys. Rev. B* **96** 224416
- [59] Senthil T, Vishwanath A, Balents L, Sachdev S and Fisher M P A 2004 *Science* **303** 1490–1494
- [60] Senthil T, Balents L, Sachdev S, Vishwanath A and Fisher M P A 2004 *Phys. Rev. B* **70** 144407
- [61] We use the program package CCCM of D. J. J. Farnell and J. Schulenburg, see <http://www-e.uni-magdeburg.de/jschulen/ccm/index.html>
- [62] Mila F 2000 *Eur. J. Phys.* **21** 499–510
- [63] Bernu B and Lhuillier C 2015 *Phys. Rev. Lett.* **114** 057201